Computational modeling of effective Young's modulus of fullerene molecules: a combined molecular dynamics simulation and continuum shell model

Esmaeal Ghavanloo*, Razie Izadi, Ali Nayebi

School of Mechanical Engineering, Shiraz University, Shiraz 71963-16548, Iran

Abstract

Estimation of the Young's modulus of structures in the nanometer size range is a difficult task. A reliable determination of this parameter is of significance in both basic and applied research. In this study, by combining the molecular dynamics (MD) simulations and continuum shell theory, we design a new approach to determine the Young's modulus of different spherical fullerenes. The results indicate that the Young's modulus of the fullerene molecules decreases nonlinearly with increasing the molecule size and understandably tents to the Young's modulus of an ideally flat graphene sheet. To the best of our knowledge, a combined atomistic-continuum method which can predict the Young's modulus of the fullerene molecules with high precision has not been provided hitherto. We believe that the present study is likely to fill the gap.

Keywords: Fullerene; Young's modulus; Molecular dynamics simulation; Continuum shell theory; Equivalent elastic stiffness

1. Introduction

Carbon-based nanoscopic structures have occupied the center stage in pure and applied research due to their extensive applications in various fields of nanoscience, nanotechnology and biotechnology [1]. Fullerene molecules are one of the earliest discovered carbon-based nanoscopic structures and they have promoted a revolution in science and technology, and they are utilized in making new devices as well as leading to new technologies. Understanding the mechanical properties of these nanoscopic structures is a necessary requirement for an efficient and accurate design of nanodevices with a predictable behavior [2]. Accordingly, the development of well-understood theoretical, computational and experimental frameworks for characterizing the mechanical

*Corresponding author.

Tel.: +98-7136133251, Fax: +98 7136473511

E-mail: ghavanloo@shirazu.ac.ir (E. Ghavanloo)

structure and behaviour of the fullerene molecules is very desirable, and it poses a huge number of challenges for researchers in this field.

Since measurement of the mechanical properties of the carbon-based nanoscopic structures is a time consuming and rather expensive endeavour, significant efforts have been invested to explore their properties and behavior through various types of simulation models including molecular dynamics (MD) simulation, continuum models and combination of atomistic simulations with continuum theories [3-7].

Compared to the mechanical properties of carbon nanotube and graphene sheet, Young's modulus of the fullerenes is much less studied. Furthermore, most researchers have utilized the mechanical properties of the graphene sheet to explore the mechanical characteristics of the fullerenes [8-11]. A noticeable gap in current research has been the lack of a model to determine the Young's modulus of the fullerene molecules. The first contribution to predict the bulk modulus of C_{60} was made by Ruoff and Ruoff [12, 13]. Compressive mechanical properties of C_{60} fullerene molecule at different temperatures have been studied by Shen [14] using Tersoff-type potential-based MD simulation. He also investigated the compressive mechanical properties of different fullerene molecules including C_{20}, C_{60}, C_{80} and C_{180} using a quantum MD simulation [15]. Giannopoulos et al. [16] studied the radial elastic stiffness of different fullerene molecules on the basis of structural mechanics spring-based method. They found that the radial Young's modulus decreases non-linearly with increasing the radius of fullerene. Recently, the elastic modulus of C_{60} molecule has been calculated by Jamal-Omidi et al. [17] using the finite element method. They modeled the fullerene structures by shell elements and the elastic properties of shell elements was adopted from graphene sheets.

Based on the above literature review, it is clear that the values of the Young's modulus of the fullerene molecules are not predicted systematically. Therefore, it is a key issue to propose a useful method which can predict the Young's modulus of different fullerenes. Motivated by this idea, in this paper, we use a combination of MD simulation and continuum shell theory to predict the effective Young's modulus of nine different spherical fullerenes, ranging from C_{60} to C_{2000}. In this connection, to find the effective Young's modulus of the fullerene molecules, the strain energy due to uniform tensile load is calculated from the MD simulation. Then, a continuum spherical shell model, according to the Flugge-type shell equations [18], is implemented to find the relation between the strain energy and tensile load. Based on the energy equivalence between the MD simulation and the continuum spherical shell model, the effective Young's modulus of the fullerenes are computed. Here, we use the large-scale atomic/molecular massively parallel simulator (LAMMPS) software [19] and Adaptive Intermolecular

Reactive Empirical Bond Order (AIREBO) force field to model the internal interactions among carbon atoms in our MD simulations to obtain the strain energy.

The organization of this paper is as follows. Details of the continuum shell model and MD simulation are discussed in Section 2. The numerical results and discussion are explained in Section 3 and Closing observations are provided in Section 4.

2. Modeling and simulation

2.1. Continuum shell theory

The mechanical behavior of a spherical fullerene can be modeled by a thin-walled shell. The spherical shell is assumed to have mean radius a and effective wall thickness t. To develop an elastic shell model, we assume that the thickness of shell remains constant during the deformation. Furthermore, it is assumed that the shell is homogeneous and isotropic with Young's modulus E and Poisson's ratio v. The atomistic structure of C_{60} molecule and its equivalent continuum-based model subjected to uniform tensile load are shown in Fig. 1. As depicted in Fig. 1, the uniform tensile load is applied by uniform displacement on the upper hexagonal face (red color), while the lower hexagonal face (yellow color) is kept fixed. These two hexagonal faces should be exactly opposite of each other to avoid asymmetric distortions.

Figure 2 shows the corresponding spherical coordinate system, though only a semicircle is considered due to symmetry of geometry and loading. Hence, the meridian angle, φ, is employed as the only independent variable. The axisymmetric governing equations for the thin-walled spherical shell are given by [18]

$$\frac{\partial}{\partial\varphi}\left(N_\varphi \sin\varphi\right) - N_\theta \cos\varphi - Q_\varphi \sin\varphi = 0 \tag{1}$$

$$\frac{\partial}{\partial\varphi}\left(Q_\varphi \sin\varphi\right) + N_\theta \sin\varphi - N_\varphi \sin\varphi = 0 \tag{2}$$

$$\frac{\partial}{\partial\varphi}\left(M_\varphi \sin\varphi\right) - M_\theta \cos\varphi - aQ_\varphi \sin\varphi = 0 \tag{3}$$

where N_φ and N_θ are membrane resultants, M_φ and M_θ are resultant bending moments and Q_φ is resultant shear force. The stress resultants are defined as integrals of stress over the thickness of a shell element. The membrane and bending moment resultants are defined as

$$N_\varphi = \frac{Et}{a(1-\nu^2)}\left[\frac{\partial u}{\partial\varphi} + w + \nu\left(u\cot\varphi + w\right)\right] \tag{4}$$

$$N_\theta = \frac{Et}{a(1-\nu^2)}\left[u\cot\varphi + w + \nu\left(\frac{\partial u}{\partial \varphi} + w\right)\right] \tag{5}$$

$$M_\varphi = \frac{Et^3}{12a(1-\nu^2)}\left[\frac{\partial \chi}{\partial \varphi} + \nu\chi\cot\varphi\right] \tag{6}$$

$$M_\theta = \frac{Et^3}{12a(1-\nu^2)}\left[\chi\cot\varphi + \nu\frac{\partial \chi}{\partial \varphi}\right] \tag{7}$$

in which u and w are meridional and radial displacements respectively, and χ is defined as

$$\chi = \frac{1}{a}\left(\frac{dw}{d\varphi} - u\right) \tag{8}$$

Equations (1)-(7) must be solved simultaneously to obtain the stress resultants N_φ, N_θ, M_φ, M_θ, Q_φ, and the displacement u, w, χ. This set of equations are reduced to the following equations for Q_φ, and χ.

$$\frac{d^2Q_\varphi}{d\varphi^2} + \frac{dQ_\varphi}{d\varphi}\cot\varphi - Q_\varphi\cot^2\varphi + \nu Q_\varphi = -Et\chi \tag{9}$$

$$\frac{d^2\chi}{d\varphi^2} + \frac{d\chi}{d\varphi}\cot\varphi - \chi\cot^2\varphi - \nu\chi = \frac{12a^2(1-\nu^2)}{Et^3}Q_\varphi \tag{10}$$

The details of mathematical derivations have been reported in Ref. [18]. The appropriate solution for coupled equations for Q_φ and χ is [18]

$$Q_\varphi = P(C_1z_1 + C_2z_2 + C_3z_3 + C_4z_4)\sin\varphi \tag{11}$$

$$\chi = \frac{P}{Et}[C_1(2\mu^2z_3 - \nu z_1) + C_2(2\mu^2z_4 - \nu z_2) - C_3(2\mu^2z_1 + \nu z_3) - C_4(2\mu^2z_2 + \nu z_4)]\sin\varphi \tag{12}$$

where the four constants C_i (i = 1, 2, 3, 4) can be evaluated uniquely by applying four proper boundary conditions. The following boundary conditions were imposed:

a) The motion of the upper hexagonal face is restricted in the z direction and the radius of mentioned hexagonal ring is fixed. This leads

$$a\varepsilon_\theta(\varphi_0) = u(\varphi_0)\cot\varphi_0 + w(\varphi_0) = 0 \tag{13a}$$

b) At $\varphi = \varphi_0$ the bending stress resultant must be zero because of the free circular cutout. Therefore, the condition is given by

$$M_\varphi(\varphi = \varphi_0) = 0 \tag{13b}$$

c) The symmetry with respect to the x-axis imposes the following boundary conditions

$$\chi(\varphi=\frac{\pi}{2})=0 \qquad Q_{\varphi}(\varphi=\frac{\pi}{2})=0 \tag{13c}$$

It should be noted that the value of φ_0 is obtained on the basis of fullerene's geometry. Furthermore, z_1, z_2, z_3 and z_4 are the solutions of hypergeometric equations (9) and (10). The parameter μ is defined by

$$\mu^4=3(1-\nu^2)\frac{a^2}{t^2}-\frac{\nu^2}{4} \tag{14}$$

The total strain energy for a spherical shell can be divided into stretching and bending contributions, $U=U_s+U_b$. The stretching energy can be written as

$$U_s=\frac{1}{2Et}\int_S (N_{\varphi}^2+N_{\theta}^2-2\nu N_{\varphi}N_{\theta})dS \tag{15}$$

where N_{φ} and N_{θ} are induced by uniform tensile load P. The membrane resultants can be expressed in terms of resultant shear force, Q_{φ}, i.e.,

$$N_{\varphi}=-Q_{\varphi}\cot\varphi-\frac{P}{2\pi a\sin^2\varphi} \tag{16}$$

$$N_{\theta}=-\frac{dQ_{\varphi}}{d\varphi}\cot\varphi+\frac{P}{2\pi a\sin^2\varphi} \tag{17}$$

In addition, the bending energy is given by

$$U_b=\frac{Et^3}{24a^2(1-\nu^2)}\int_S [\left(\frac{d\chi}{d\varphi}\right)^2+(\chi\cot\varphi)^2+2\nu\chi\frac{d\chi}{d\varphi}\cot\varphi]dS \tag{18}$$

It is clear that the total strain energy can be calculated when two parameters Q_{φ} and χ are appropriately obtained from equations (11) and (12). By using equations (11), (12), (15) and (18), and after very lengthy derivations, the total strain energy can be obtained as

$$U=\frac{1}{2}\frac{P^2}{E}C_u \tag{19}$$

where

$$C_u=\int_S H(\varphi,a,t,\nu)dS=4\pi a^2\int_{\varphi_0}^{\frac{\pi}{2}} H(\varphi,a,t,\nu)\sin^2\varphi\, d\varphi \tag{20}$$

The function H can be defined as

$$
\begin{aligned}
H(\varphi,a,t,\nu) = \frac{1}{t}[&((C_1z_1+C_2z_2+C_3z_3+C_4z_4)\cos\varphi+\frac{1}{2\pi a\sin^2\varphi})^2 \\
&+(\frac{1}{2\pi a\sin^2\varphi}-\cot\varphi\frac{d}{d\varphi}((C_1z_1+C_2z_2+C_3z_3+C_4z_4)\sin\varphi))^2 \\
&+2\nu((C_1z_1+C_2z_2+C_3z_3+C_4z_4)\cos\varphi+\frac{1}{2\pi a\sin^2\varphi})(\frac{1}{2\pi a\sin^2\varphi}-\cot\varphi\frac{d}{d\varphi}((C_1z_1+C_2z_2+C_3z_3+C_4z_4)\sin\varphi))] \\
&+\frac{t}{12a^2(1-\nu^2)}[(\frac{d}{d\varphi}((C_1(2\mu^2z_3-\nu z_1)+C_2(2\mu^2z_4-\nu z_2)-C_3(2\mu^2z_1+\nu z_3)-C_4(2\mu^2z_2+\nu z_4))\sin\varphi))^2 \\
&+((C_1(2\mu^2z_3-\nu z_1)+C_2(2\mu^2z_4-\nu z_2)-C_3(2\mu^2z_1+\nu z_3)-C_4(2\mu^2z_2+\nu z_4))\cos\varphi)^2 \\
&+2\nu((C_1(2\mu^2z_3-\nu z_1)+C_2(2\mu^2z_4-\nu z_2)-C_3(2\mu^2z_1+\nu z_3)-C_4(2\mu^2z_2+\nu z_4))\cos\varphi) \\
&\times\frac{d}{d\varphi}((C_1(2\mu^2z_3-\nu z_1)+C_2(2\mu^2z_4-\nu z_2)-C_3(2\mu^2z_1+\nu z_3)-C_4(2\mu^2z_2+\nu z_4))\sin\varphi)]
\end{aligned}
\tag{21}
$$

Furthermore, for small deformations, the total strain energy of the system is expressed as

$$
U=\frac{1}{2}\frac{P^2}{K}=\frac{1}{2}K\delta^2 \tag{22}
$$

wherein δ is deformation and K denotes elastic stiffness and it can be determined from the MD simulations. Therefore, the Young's modulus of the spherical fullerene is obtained as

$$
E=K\int_S H(\varphi,a,t,\nu)dS \tag{23}
$$

2.2. Molecular dynamics simulation

In this paper, MD simulations are carried out using LAMMPS code [19], a massively parallel MD simulator from Sandia National Laboratories and the results are visualized using VMD package [20]. It has been shown that the Adaptive Intermolecular Reactive Empirical Bond Order (AIREBO) potential can accurately compute the bond-bond interaction, bond breaking, and bond reforming in the carbon atoms [21]. Furthermore, this force field has been proven to be reliable for reproducing the mechanical behavior observed experimentally in the fullerenes [22, 23]. Hence, the AIREBO potential is used here to model the interactions among carbon atoms in the fullerene. According to this model, the total potential energy of the system is given by [24, 25]

$$
E_{AIREBO}=\frac{1}{2}\sum_i\sum_{j\neq i}\left(E_{ij}^{REBO}+E_{ij}^{LJ}+\sum_{k\neq i,j}\sum_{l\neq i,j,k}E_{kijl}^{Tors}\right) \tag{23}
$$

where E^{REBO} shows the second generation of REBO potential proposed by Brenner et al [25], E^{Tor} is torsional potential due to dihedral rotation of bonds and E^{LJ} is potential associated with the long range non-bonded interaction among atoms. Detailed explanation about the terms of the AIREBO potential can be found in Refs. [24, 25].

We first create the initial geometries of several near-spherical fullerenes including C_{60}, C_{180}, C_{240}, C_{540}, C_{720}, C_{980}, C_{1280}, C_{1620} and C_{2000}. Prior to deformation, the geometric structure of the fullerenes must be relaxed to

achieve stress-free state. Since all fullerenes are not perfectly sphere, a fullerene may be treated as a sphere with the equivalent radius a. It was shown that, for the fullerenes with more than 100 atoms, the difference between the area of the fullerene and its equivalent sphere is less than one percent [26]. Table 1 gives the equivalent radius for the fullerenes based on the position of atoms after relaxation. To ensure quasi-static deformation, rate of deformation should be small. In this way, we implement the deformation-control method by applying the velocity 0.01 Å/s to the upper hexagonal face of the fullerene.

The velocity Verlet algorithm [27] is used to integrate the equations of motion with a time step 1 fs. This time step guarantees good conservation of energy [28]. The Nosé–Hoover thermostat [29] is used to maintain the simulation temperature at T = 300 K. The use of this thermostat leads to less fluctuations in the temperature [30]. Furthermore, to ensure constant volume and temperature, we apply a NVT ensemble for the MD simulations with a shrink-wrap boundary condition at a constant temperature. The conjugate gradient algorithm is applied to determine the stress-free minimum-energy prior to dynamics simulation.

3. Results and discussion

In this section, we show the applicability of the present formulations and simulations for predicting the effective Young's modulus of the fullerene molecules. During tensile test simulations, we recorded the deformation and the potential strain energy of the fullerenes. The potential strain energy versus deformation curves for C_{60} and C_{180} fullerene molecules are shown in Fig. 3. It is observed from Fig.3 that, for small deformation, the potential energy of simulated fullerenes increases almost quadratically with respect to deformation. By fitting equation (21) to the MD simulation results, we can obtain the equivalent elastic stiffness for different spherical fullerenes. The calculated equivalent elastic stiffness of the fullerenes with different radii is depicted in Fig. 4. As expected, the equivalent elastic stiffness is found to decrease as the number of atoms increases. Furthermore, the results from MD simulations can be well-captured by using the following relation

$$K = \frac{2340}{a^{1.59}} \tag{24}$$

Implementing the values of equivalent elastic stiffness from the MD simulation and using equation (11), the Young's modulus of each fullerene is calculated. To obtain the value of the integral presented in equation (22), the Poisson ratio and effective wall thickness have to be chosen appropriately. In this study, it is assumed that the Poisson ratio remains constant for fullerenes with different radii, Therefore, all simulations are performed with the Poisson ratio of 0.3 [31]. The effective wall thickness is an ambiguous parameter and the exact value of the wall thickness of the fullerenes has not been completely clarified in the literature, and a set of values ranging from

0.06 to 0.34 nm have been adopted in the several studies. It is well-known that different values of this parameter, would lead to different values for the Young's modulus. Here, we have proposed a necessary condition (but not sufficient) for justifying an effective thickness of fullerene. It is well known that the surface of a fullerene molecule contains only a number of atoms and that the forces in the fullerene are transmitted through these atoms. However, in a continuum shell model the same forces are transmitted through a continuous wall. Hence, the effective wall thickness of molecule cannot be greater than or equal to the atomic thickness (≈ 0.1 to 0.2 nm). Based on this point, the assumed value of 0.34 nm, as well as those larger than 0.2 nm should be excluded in future investigations. Therefore, in our numerical calculation, we use t = 0.182 nm which is satisfy the above criterion and also has been adopted in previous studies [32, 33].

Figure 5 displays the calculated Young's modulus as a function of the equivalent radii of the fullerenes. For the sake of comparison, the results given by Giannopoulos et al. [16] on the basis of structural mechanics are also presented in Fig. 5. We note that the comparison is reasonable. This indicates that the proposed method in this work provides accurate results. As expected, it is found that the Young's modulus is a decreasing function of the radius and it converges gradually to the Young's modulus of ideally flat graphene. However, the fullerene C_{60} shows an irregular result. It is worth noticing that the appearance of irregularity in the Young's modulus is attributed to the assumption of thin-walled shell theory. Therefore, it can be concluded that thin shell theory is not applicable for the case of small fullerenes. Furthermore, as can be expected, the Young's modulus of fullerenes approaches to the Young's modulus of graphite when the diameter is large.

4. Conclusions

In conclusion, a combination of molecular dynamics simulation and elastic shell theory was used to calculate the Young's modulus of the spherical fullerenes. To our knowledge, this is the first time that the Young's modulus of the fullerene molecules is predicted systematically on the basis of a combined atomistic-continuum method. It may be considered as a valuable task for modeling these nanoscopic structures in future works. To this end, both MD simulations and elastic thin shell theory were utilized to simulate the tensile test of the fullerenes. A quadratic relationship was obtained between the strain energy and the deformation in both MD simulation and continuum solution. Using this relationship, we obtained the equivalent elastic stiffness and Young's modulus for different spherical fullerenes. Furthermore, our results compares reasonably with previous data. Finally, it is worth noticing that the proposed method is applicable to the investigation of the Young's modulus of other shell-like spherical nanoscopic structures.

Compliance with ethical standards

Conflicts of interest The authors declare that there are no conflicts of interest.

References

[1] H.J. Fecht, K. Brühne, P. Gluche, Carbon-based Nanomaterials and Hybrids: Synthesis, Properties, and Commercial Applications, Pan Stanford Publishing, Singapore, 2014.

[2] H. Rafii-Tabar, E. Ghavanloo, S.A. Fazelzadeh, Nonlocal continuum-based modeling of mechanical characteristics of nanoscopic structures, Phys. Rep. 638 (2016) 1-97.

[3] A. Montazeri, M. Sadeghi, R. Naghdabadi, H. Rafii-Tabar, Multiscale modeling of the effect of carbon nanotube orientation on the shear deformation properties of reinforced polymer-based composites, Phys. Lett. A 375 (2011) 1588-1597.

[4] C. Baykasoglu, A. Mugan, Coupled molecular/continuum mechanical modeling of graphene sheets, Physica E 45 (2012) 151-161.

[5] S. Rouhi, Y. Alizadeh, R. Ansari, On the elastic properties of single-walled carbon nanotubes/poly(ethylene oxide) nanocomposites using molecular dynamics simulations, J. Mol. Model. 22 (2016) 41.

[6] E. Ghavanloo, S.A. Fazelzadeh, H. Rafii-Tabar, A computational modeling of Raman radial breathing-like mode frequencies of fullerene encapsulated inside single-walled carbon nanotubes, J. Mol. Model. 23 (2017) 48.

[7] F. Mehralian, Y. Tadi Beni, Molecular dynamics analysis on axial buckling of functionalized carbon nanotubes in thermal environment, J. Mol. Model. 23 (2017) 330.

[8] D. Kahn, K.W. Kim, M.A. Stroscio, Quantized vibrational modes of nanospheres and nanotubes in the elastic continuum model, J. Appl. Phys. 89 (2001) 5107.

[9] K. Behfar, R. Naghdabadi, Nanoscale modeling of an embedded multi-shell fullerene and its application to vibrational analysis, Int. J. Eng. Sci. 44 (2006) 1156-1163.

[10] S. Adhikari, R. Chowdhury, Vibration spectra of fullerene family, Phys. Lett. A 375 (2011) 2166-2170.

[11] E. Ghavanloo, S.A. Fazelzadeh, Nonlocal shell model for predicting axisymmetric vibration of spherical shell-like nanostructures, Mech. Adv. Mater. Struc. 22 (2015) 597-603.

[12] R.S. Ruoff, A.L. Ruoff, Is C60 stiffer than diamond? *Nature* 350 (1991) 663-664.

[13] R.S. Ruoff, A.L. Ruoff, The bulk modulus of C_{60} molecules and crystals: a molecular mechanics approach, Appl. Phys. Lett. 59 (1991) 1553-1555.

[14] H. Shen, The compressive mechanical properties of C_{60} and endohedral $M@C_{60}$ (M =Si, Ge) fullerene molecules, Mater. Lett. 60 (2006) 2050-2054.

[15] H. Shen, The compressive mechanical properties of C_n (n = 20, 60, 80, 180) and endohedral $M@C_{60}$ (M = Na, Al, Fe) fullerene molecules, Mol. Phys. 105 (2007) 2405-2409.

[16] G.I. Giannopoulos, S.K. Georgantzinos, P.A. Kakavas, N.K. Anifantis, Radial stiffness and natural frequencies of fullerenes via a structural mechanics spring-based method, Fuller. Nanotub. Car. N. 21 (2013) 248-257.

[17] M. Jamal-Omidi, M. ShayanMehr, R. Rafiee, A study on equivalent spherical structure of buckyball-C_{60} based on continuum shell model, Lat. Am. J. Solids Stru. 13 (2016) 1016-1029.

[18] W. Flugge, Stresses in Shells, Springer-Verlag, Berlin, 1960.

[19] P. Steve, P. Crozier, A. Thompson, LAMMPS-large-scale atomic/molecular massively parallel simulator, Sandia Natl. Lab. (2007) 18.

[20] W. Humphrey, A. Dalke, K. Schulten, VMD: visual molecular dynamics, J. Mol. Graph. 14 (1996) 33-38.

[21] K. Min, N.R. Aluru, Mechanical properties of graphene under shear deformation, Appl. Phys. Lett. 98 (2011) 013113.

[22] H. Nejat Pishkenari, A. Nemati, A. Meghdari, S. Sohrabpour, A close look at the motion of C_{60} on gold, Curr. Appl. Phys. 15 (2015) 1402-1411.

[23] H. Nejat Pishkenari, P. Ghaf Ghanbari, Vibrational properties of C_{60}: a comparison among different inter-atomic potentials, Comp. Mater. Sci. 122 (2016) 38-45.

[24] S.J. Stuart, A.B. Tutein, J.A. Harrison, A reactive potential for hydrocarbons with intermolecular interactions, J. Chem. Phys. 112 (2000) 6472-6486.

[25] D.W. Brenner, O.A. Shenderova, J.A. Harrison, S.J. Stuart, B. Ni, S.B. Sinnott, A second-generation reactive empirical bond order (REBO) potential energy expression for hydrocarbons, J. Phys: Condens. Matter 14 (2002) 783-802.

[26] Y. Wei, B. Wang, J. Wu, R. Yang, M.L. Dunn, Bending rigidity and Gaussian bending stiffness of single-layered graphene, Nano Lett. 13 (2012) 26-30.

[27] M.P. Allen, D.J. Tildesley, Computer Simulation of Liquids, Oxford: Clarendon Press, 1987.

[28] C.L. Zhang, H.S. Shen, Thermal buckling of initially compressed single-walled carbon nanotubes by molecular dynamics simulation, Carbon 45 (2007) 2614-2620.

[29] W.G. Hoover, Canonical dynamics: Equilibrium phase-space distributions, Phys. Rev. A 31 (1985) 1695.

[30] C.L. Zhang, H.S. Shen, Predicting the elastic properties of double-walled carbon nanotubes by molecular dynamics simulation, J. Phys. D: Appl. Phys. 41 (2008) 055404.

[31] V.M. Levin, V.D. Blank, V.M. Prokhorov, J.M. Soifer, N.P. Kobelev, Elastic modules of solid C_{60}: measurement and relationship with nanostructure, J. Phys. Chem. Solids 61 (2000) 1017-1024.

[32] L. Chadderton, Axisymmetric vibrational modes of fullerene C_{60}, J. Phys. Chem. Solids 54 (1993) 1027-1033.

[33] S. Ahmad, Continuum elastic model of fullerenes and the sphericity of the carbon onion shells, J. Chem. Phys. 116 (2002) 3396-3400.

Table 1. Calculated Radius for Some Spherical Fullerenes

atoms (*N*)	Radius (Å)
60	3.549
180	6.042
240	6.960
540	10.361
720	11.940
980	13.921
1280	15.896
1620	17.873
2000	19.853

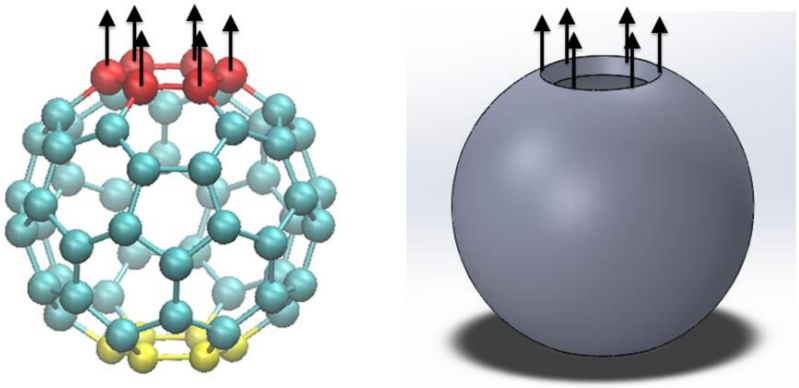

Fig. 1. Molecular structure of C_{60} fullerene and its equivalent beam model subjected to uniform tensile load.

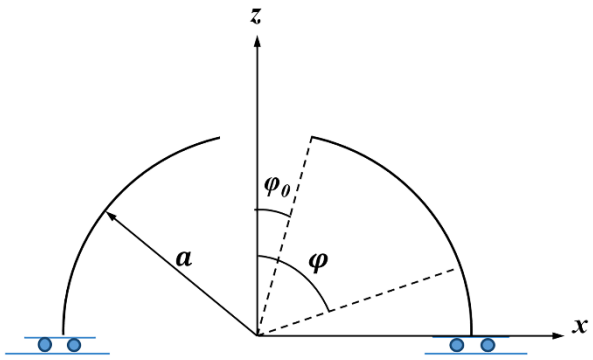

Fig. 2. Sketch of coordinate system for a spherical shell.

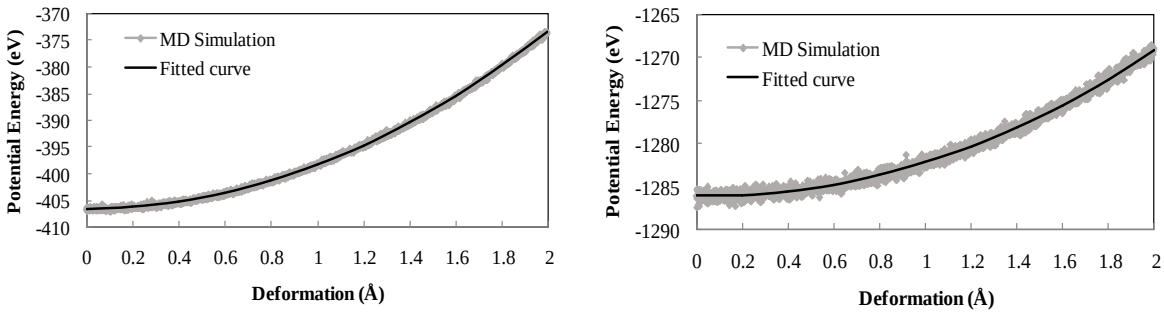

Fig. 3. Variations of the potential energy with the deformation. (a) C_{60} fullerene. (b) C_{180} fullerene.

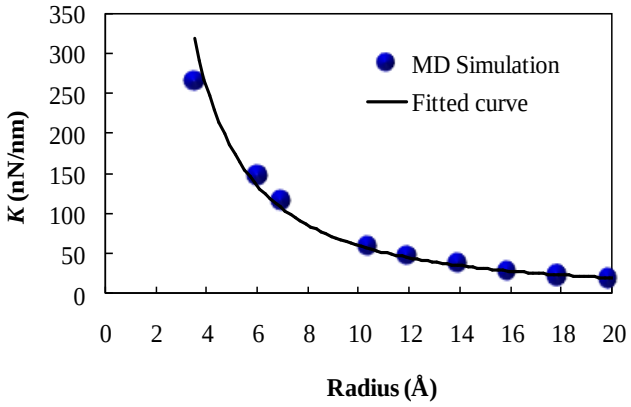

Fig. 4. The equivalent elastic stiffness as a function of radius of the fullerene. Here, the solid circles correspond to the results calculated from MD simulations.

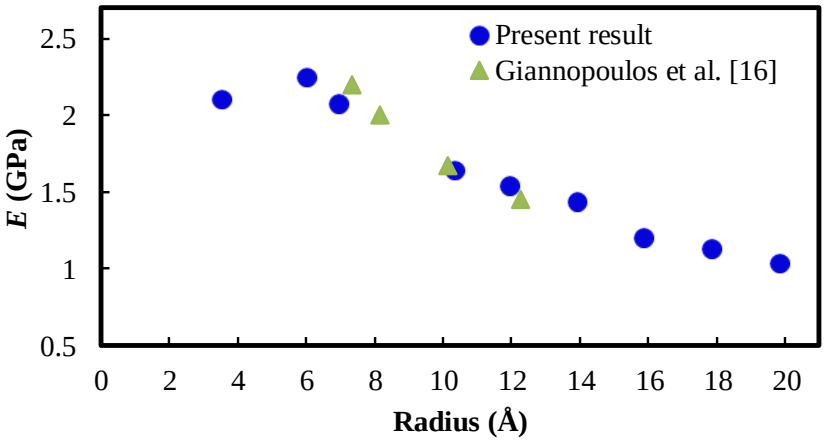

Fig. 5. Predicted Young's modulus of fullerenes with different radii.